12A.4

Land-surface response to shallow cumulus

FABIENNE LOHOU*
Laboratoire d'Aérologie, Université de Toulouse, Campistrous, France

EDWARD G. PATTON
National Center for Atmospheric Research, Boulder, CO, USA

1. Introduction

Cloud feedbacks in the climate system are a major source of uncertainty in model projections of global warming (Stephens, 2005). Analysis of satellite data (Hartmann et al., 1992) and climate models (*e.g.,* Slingo, 1990; Bony and Dufresne, 2005; Webb et al., 2006) suggests that much of this uncertainty is associated with low clouds. From the climate point of view, low/shallow clouds are most principally distinct from deep/tall and high clouds through the temperature difference (ΔT) between cloud top (T_c) and the surface (T_s); of importance is that the emissivity effect of clouds increases with an increase in ΔT, and their albedo affect need not, hence perturbations to properties of low clouds disproportionately affect albedo and the net radiative balance of the system as a whole (Stevens and Brenguier, 2009).

Due to their relatively small size and radiative impact, and their tendency not to produce rain, shallow cumulus clouds have received much less attention within the scientific community than the myriad of other cloud forms (*i.e.,* stratocumulus, deep precipitating convection, etc) (Stevens, 2005). That said, a significant portion of the research has focused on understanding and parameterizing the transport and mixing associated with shallow cumulus and their roots within the subcloud layer (*e.g.,* LeMone and Pennell, 1976; Nicholls and LeMone, 1980; Nicholls et al., 1982; Teidtke et al., 1988; Siebesma, 1998; Brown et al., 2002; Soares et al., 2004; Bellon and Stevens, 2005; Zhao and Austin, 2005a,b; Stevens, 2007; Bretherton and Park, 2008; Heus and Jonker, 2008; Stechmann and Stevens, 2010, among numerous others). However, eventhough the impact of cumulus convection on surface fluxes has been shown to significantly affect larger-scale circulations and the skill of medium-range weather forecasts (Tiedtke, 1989), the coupling between shallow cumulus and the land surface has received very little attention.

Ascertaining the impact of shallow cumulus clouds on surface fluxes using in-situ observations is extremely difficult because the sample duration can be relatively short. Factors affecting this duration include: 1) short lifetimes ($\sim$ 10 minutes) of individual clouds, 2) the small horizontal scales ($\sim$ 1 km) of the clouds, and 3) the potentially short time which any particular cloud spends overhead. We therefore turn to turbulence-resolving calculations.

Large-eddy simulation (LES) largely began with Deardorff (1970) and has progressed over the last few decades to become a close counterpart to outdoor observations. Most LES studies of cloudy boundary layers have focused on the cloud response to variations in imposed surface forcing (*e.g.,* Nicholls et al., 1982; Lewellen and Lewellen, 1996; Moeng, 1998, 2000; Brown et al., 2002; Lewellen and Lewellen, 2002; Siebesma et al., 2003; Zhu and Albrecht, 2003; Stevens, 2007 among others). Although a few researchers have investigated low clouds using turbulence resolving calculations with coupled land surfaces (*e.g.,* Deardorff, 1980; Golaz, 2001; Jiang and Feingold, 2006), these efforts focused on the cloud response to spatially varying surface forcing. Very little effort, if any, has emphasized the local surface response to shallow cumulus passing overhead.

Using a similar toolset as Deardorff (1980), Golaz (2001) and Jiang and Feingold (2006) but using Brown et al.'s (2002) initial conditions and forcing as our basis (where the case's details are described in §2.), we investigate the interactions surrounding the coupling between shallow cumulus and the land surface. As depicted in Fig. 1, these interactions define the outline of this paper.

Passing shallow cumulus clouds briefly and intermittently reduce the solar irradiance. The surface responds by rapidly adjusting the balance between sensible, latent and soil heat flux. Precisely how the surface partitions the available energy among these fluxes remains unclear; the average and local surface response are both investigated in §3. (Fig. 1, point I). Three processes likely modify the surface energy balance (SEB): 1) the reduction of incoming solar radiation, 2) the modification of surface fluxes resulting from cloud-induced atmospheric turbulence and generation of secondary circulations, and 3) the warming and drying of the boundary layer by entrainment of free tropospheric air into the boundary layer altering the SEB by modifying temperature and moisture gradients

*Corresponding address: Fabienne Lohou, Laboratoire d'Aérologie, Université de Toulouse, and CNRS, 8 route de Lannemezan, 65300 Campistrous, France. E-mail: Fabienne.Lohou@aero.obs-mip.fr

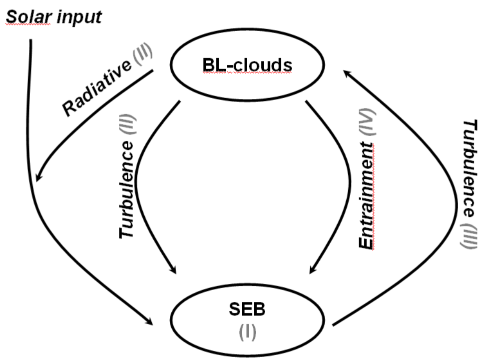

Figure 1: Interactions involved in the coupling between the surface energy balance (SEB) and boundary-layer clouds (BL-clouds). (I) The average and local surface response to shallow cumulus. (II) The effects of decreasing solar input and cloud-induced turbulence on the SEB. (III) The boundary layer's response to cloud-induced surface heterogeneity. (IV) Entrainment at boundary layer top with shallow cumulus.

between the atmosphere and the skin surface. The relative importance of cloud-induced solar irradiance vs. turbulence modifications on the SEB (Fig. 1, point II) is not developed in this extended abstract. The atmospheric boundary layer's response to cloud-induced surface flux heterogeneity and the impact on cloud roots are investigated in §4. (Fig. 1, point III), shallow-cumulus modification to PBL entrainment rates are discussed in §5. (Fig. 1, point IV), and §6. summarizes the results and presents some concluding remarks.

2. Coupled model and case description

The simulated case is based on observations from the Atmospheric Radiation Measurement (ARM) Southern Great Plain (SGP) central facility on June 21, 1997. The initial atmospheric conditions come from those defined for Brown et al.'s (2002) large eddy simulation intercomparison study. In the Brown et al. (2002) study, initial profiles of potential temperature (θ), total water mixing ratio (r_v) and horizontal winds were prescribed at 0530 Local Solar Time (LST) corresponding to 1130 Universal Time Coordinate (UTC). To account for significant cooling between 0530 and 0730 LST (not accounted for in the large scale forcings) and to prevent any clouds to reach the the top of the simulated domain, the initial profiles were slightly idealized compared to those observed (Brown et al., 2002). These initial θ and r_v profiles are presented in Fig. 3c and d. Vertical profiles of the horizontal wind are initially constant with height (u = 10 m s^{-1} and v = 0 m s^{-1}), and a 10 m s^{-1} westerly geostrophic wind is imposed throughout the simulation. Large scale heat and moisture advection follow those defined by Brown et al. (2002).

In the simulation discussed here, Brown et al.'s (2002) imposed surface heat and moisture fluxes are replaced by coupling the atmospheric large-eddy simulation with an interactive land-surface model (Patton et al., 2005), where a separate implementation of the NOAH land-surface model at every horizontal grid point at the bottom of the 3D turbulence resolving atmsopheric simulation uses a one-dimensional soil representation to solve an energy balance driven by the instantaneous overlying atmospheric wind, temperature, and humidity variables to determine the local instantaneous surface momentum, heat and moisture fluxes. Horizontally homogeneous initial soil temperature and soil moisture content profiles are generated by running the one-dimensional High Resolution Land Data Assimilation System (HRLDAS, Chen et al., 2007) for a six month period driven by data from the ARM SGP site. This process allows: 1) the LSM to equilibrate with the forcing, and 2) to choose the soil and vegetation types which best reproduce the ARM SGP soil temperature, moisture and surface flux measurements. It is important to note that this study does not aim to perfectly reproduce the ARM SGP surface flux observations, but rather to lean on realistic conditions when studying the interactions between shallow clouds and the underlying land surface.

The parameter combinations generating the best agreement between the HRLDAS simulated and the observed fluxes during the six month period included a clay-loam soil type with a volumetric soil moisture wilting point (SMC_{wp}) and field capacity (SMC_{fc}) of 0.103 and 0.382 m^3 m^{-3}, respectively, and a non-transpiring grass vegetation type with and albedo of 0.2 and a roughness length of 0.08 m. Initial vertical profiles of soil temperature and moisture were selected from the six-month-long HRLDAS simulation when both surface flux and atmospheric conditions were in close agreement to those observed on June 21, 1997. The soil moisture index (SMI) defined as:

$$SMI = \frac{SMC - SMC_{wp}}{SMC_{fc} - SMC_{wp}}, \qquad (1)$$

where SMC is the soil moisture content, is then equal to 0.93. Therefore the initial soil conditions are horizontally homogeneous, but the soil temperature and moisture conditions at every horizontal location freely evolve based upon local atmospheric demand.

The simulation resolves a 10.24 km^2 horizontal domain extending vertically to 4.096 km using 512^3 grid points, thereby implying horizontal and vertical grid resolutions of 20 and 8 m, respectively. The soil is resolved by four layers whose bottom limits are [0.05, 0.2, 0.6, 1] m. The simulation lasts 7.5 hours, beginning at 0530 LST ending at 1300 LST with time step determined by a Courant-

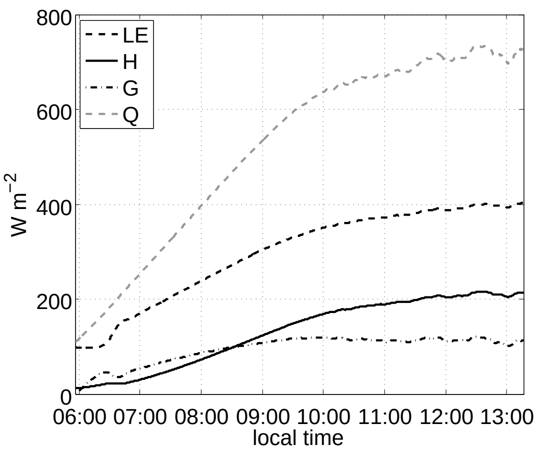

Figure 2: Temporal evolution of the surface energy balance terms (LE, H, G and Q).

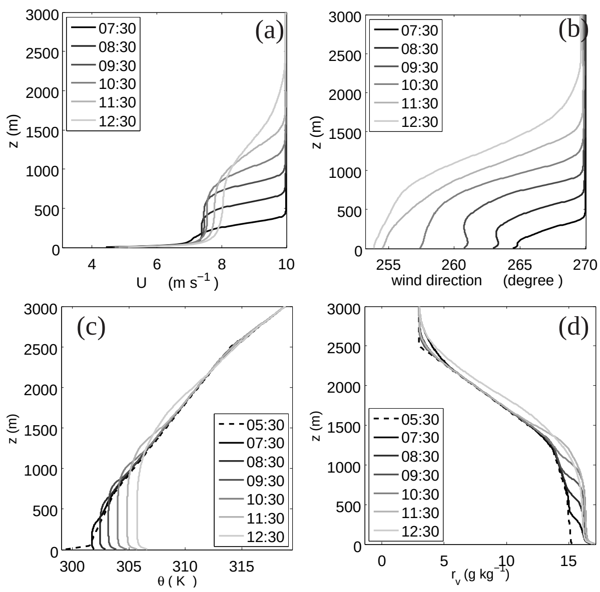

Figure 3: Mean vertical hourly profiles of: (a) mean horizontal wind - U, (b) wind direction, (c) θ, and (d) r_v between 0730 and 1230 LST. The initial vertical profiles of θ and r_v at 05:30 LST are included in (c) and (d), respectively.

Freidrichs-Lewy (CFL, Courant et al., 1967) number of 0.5. After an initial period during which the turbulence develops, the timestep averaged approximately 0.5 s.

The surface energy balance terms (net radiation: Q, sensible and latent heat flux: H and LE, and the soil heat flux: G) estimated by the LSM and averaged horizontally are presented in Fig. 2 between 0600 and 1300 LST. After the clouds begin to form (starting between 0900 and 1000 LST), the cloud shading clearly impacts net radiation (Q) throughout the rest of the simulation as depicted by Q's flattening and oscillating behaviour. At noon, H and LE are about 200 and 400 W m^{-2}, respectively, compared to 140 and 500 W m^{-2} in Brown et al. (2002).

Fig. 3 presents the evolution of mean hourly vertical profiles of the horizontal wind speed (U) and direction, potential temperature (θ) and the water vapor mixing ratio (r_v). The horizontal wind speed rapidly homogeneizes in the mixed layer (at $\sim$ 7 to 8 m s^{-1}) exhibiting strong wind shear in the surface layer and at the boundary layer top, and from 0900 LST in the cloud layer. The simulation's imposed geostrophic wind is westerly at all heights but in response to Coriolis turning and surface drag, the horizontal winds turn about 15° by the end of the simulation. Between 0600 and 1300 LST, the mean potential temperature in the mixed layer increases of 5.5 K. Despite significant surface evaporation (as quantified by LE in Fig. 2), the increase in water vapor mixing ratio increases only 1 g kg^{-1} over the same time frame; which illustrates the drying of the well-mixed boundary layer by entrainment of dry air from aloft occuring both at that PBL top and within the cloud layer. Prior to the onset of clouds, the vertical buoyancy flux profile follows the expected $\sim$ 0.2 relationship between surface and entrainment buoyancy flux as that found in clear convective boundary layers (Fig. 4, Deardorff et al., 1980). Above the mixed layer, the positive buoyancy flux values are associated with the cloud layer. The cloudy layer's development is described through the cloud fraction, the liquid water path, the cloud base and top in Fig. 5. The cloud base and top are defined hereafter by the lowest and highest non-zero values of the mean liquid water vertical profile. From 0800 to 0900 LST the cloud base and summit are defined but are not reliable since the liquid water path and the cloud fraction remain negligable. The boundary layer top z_i, estimated using the height of minimum buoyancy flux, is also depicted in Fig. 5. After 0900 LST, z_i and the cloud base match well.

The simulated cumuli are forced (**?**) but their characteristics are close to active cumuli, with 20 to 30% of cloud fraction and a vertical development to 1.5 km at 1300 LST (Fig. 5).

3. Surface response to boundary layer clouds

Land-surface response to shallow cumuli is poorly documented. Yet climate models rely on properly handling cloud-surface interactions for their lower boundary condition. Therefore, misrepresentation of these couplings can act as a source of uncertainty in climate prediction, as pointed out by Betts (2007) who studied the connection between cloud fields and both surface and large-scale processes for Mississippi River sub-basins using ERA40 reanalysis data. Identifying impacts of shallow clouds on surface fluxes experimentally usually leads to highly fluc-

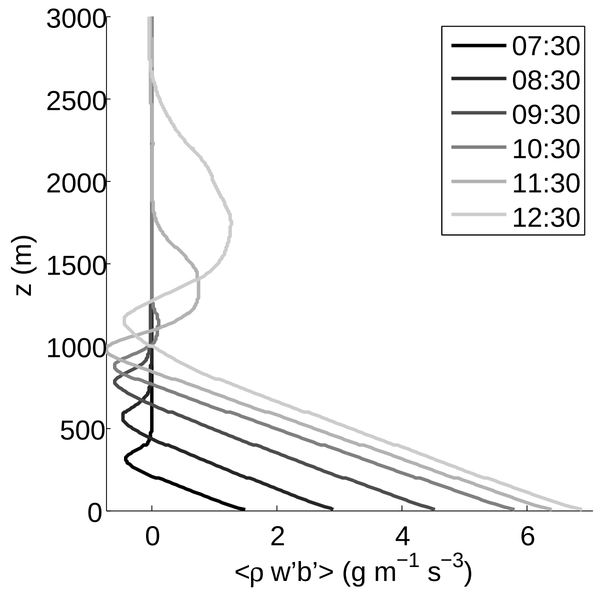

Figure 4: Time evolution of the profile of hourly-averaged buoyancy flux ($\langle \rho w'b' \rangle$).

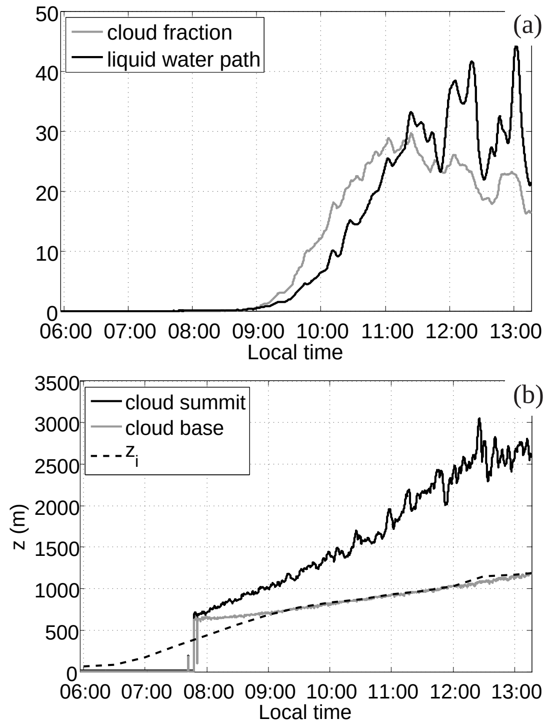

Figure 5: Temporal evolution of: (a) cloud fraction (%) and liquid water path (g m^{-2}), and (b) the cloud layer base, top, and the boundary layer height, z_i (defined as the minimum of the buoyancy flux).

tuating fluxes because cloud shading tends to last only for short periods ($\sim$ 10 minutes) within a 20 to 30 minute average making robust statistics difficult to obtain.

The combination of 1) the land-surface coupling in our simulation, and 2) the simulation domain's horizontal extent which permits numerous clouds at any given time, allows investigation of shallow clouds' impact on the surface energy balance (SEB) in two ways: 1) in a horizontally-average sense, and 2) from a local point of view. Analyzing the results in an average sense provides information on the large scale (or net) impact of cloud shading and surface forcing at regional scales. Whereas, analyzing the results locally provides information on surface's ability to react to short-duration variations in solar irradiance and to atmospheric fluid dynamics generated by the clouds.

3.1 Average surface response

In order to properly quantify the effect of shallow clouds on the continental SEB, a comparison would be necessary of two very similar boundary layers, with and without cloud. Such a comparison is difficult to perform since clouds are dynamically and thermodynamically active in PBL processes, where turning off cloud formation in the LES would dramatically change the PBL characteristics and the two boundary layers would therefore not be comparable. So in this study we solely use a cloudy simulation, where we assume that the terms in the energy balance from areas not shaded by clouds (un-shaded) are close to what they would be in a cloud-free boundary layer. This assumption presumes *a-priori* that clouds' radiatively affect surface fluxes with significanly larger magnitude than do clouds affect near-surface fluid motions.

Fig. 6 presents the temporal evolution of the SEB terms in the presence of shallow clouds compared to without clouds, where at each simulation time step the surface sensible (H), latent (LE), and soil heat flux (G), and net radiation (Q) horizontally-averaged over the entire domain are each divided by their respective value horizontally-averaged solely over the un-shaded area. This ratio quantifies how the various terms in the energy balance respond to the cloud-induced reduction in Q. At 0900 LST, the ratio for all SEB terms are 100% since the clouds have not yet developed. With increasing cloud fraction and the deepening of the cloud layer, every term in the SEB diminishes to below 100%. Between 0900 and 1200 LST, Q decreases by about 10%, which leads to a 10% and 5% decrease of H and LE, respectively. The soil heat flux decreases more than the other SEB terms (by $\sim$ 20%). Notice that the non-linear response of the surface leads to different reduction between each of the SEB terms. As a consequence, the evaporative fraction $EF = LE/(H+LE)$ increases by $\sim$ 2 to 3% in the cloudy boundary layer relative to the cloud-free boundary layer.

To establish how this result depends on soil type and

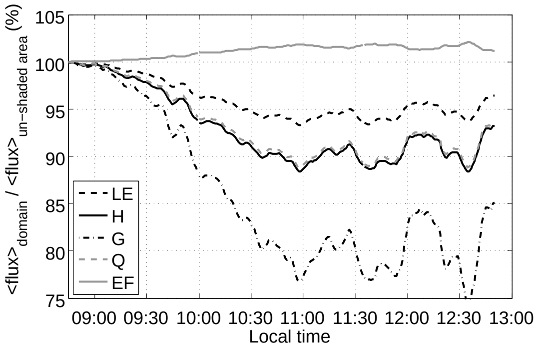

Figure 6: Temporal evolution of SEB terms (LE, H, G and Q) and evaporative fraction (EF) averaged over the domain and normalized by their average value over the un-shaded areas (in percentage).

soil moisture, simulations using the one-dimensional version of the NOAH LSM (*i.e.,* uncoupled from the LES) responding to a 10% solar irradiance reduction are investigated for three different soil types, and for widely ranging SMI. These offline tests (not shown) suggest that the 2 to 3% increase in EF observed in the coupled LES data is not dependant on SMI or soil-type.

3.2 Local surface response

Shallow clouds passing over a fixed point at the surface induces rapid changes in Q, which leads to an imbalance between the atmosphere and the surface from which the surface must recover. Fig. 7 shows a one-hour time-evolution at single surface point of the SEB terms (Fig. 7a) and of the SEB terms normalized by local net radiation Q (Fig. 7b). For clarity, the temporal resolution is about 50 s. Clouds suddenly reduce the net radiation from 800 W m^{-2} down to 200 W m^{-2}. The surface responds immediately with a rapid drop down to 50 and 200 W m^{-2} of H and LE, respectively (Fig. 7a). As previously discussed with respect to the horizontally-averaged results, the sensible heat flux decreases proportionally with the net radiation (*i.e.,* the normalized sensible heat flux remains equal to about $0.3Q$ when shallow clouds pass over head, Fig. 7b). Therefore, H reacts similarly whether considering the average or the local response. Contrary to the finding for H, LE is about $0.5Q$ in the un-shaded areas and increases to $\sim 1.3Q$ under the cloud. So, the flux density released by the shaded surface through evaporation is higher than the net radiative flux density available at the surface. The soil heat flux (G) compensates this imbalance shifting from 150 W m^{-2} (or $\sim 0.2Q$) in the un-shaded area down to -100 W m^{-2} ($\sim$ -0.5Q) when clouds are overhead (Fig. 7).

The large soil heat flux variations illuminate the key

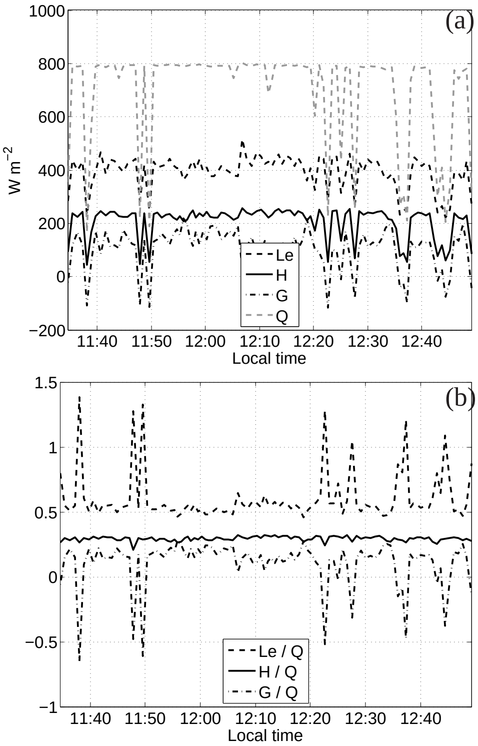

Figure 7: (a) One-hour time evolution of the SEB terms at a single grid point during the passage of a shallow cumulus cloud. (b) Same temporal evolution as (a), but H, LE and G are normalized by the local net radiation Q.

role the soil plays in determining the partitioning between sensible and latent heat flux under rapidly varying solar irradiance: $Q = LE + H + G$, with $Q = 1.2Q + 0.3Q - 0.5Q$ under the clouds, and $Q = 0.5Q + 0.3Q + 0.2Q$ in the un-shaded areas.

4. Boundary layer response to cloud-induced surface flux heterogeneity

Is the cloud-induced surface flux heterogeneity significant enough to produce an atmospheric response (Fig. 1, point III)? Although this question could be answered from a variety of view points, this section will focus on the vertical buoyancy flux.

In the subcloud layer, cloud roots are associated with well-defined strong updrafts of warmer and moister air than in the surroundings (Lohou et al., 1998). An example cloud root from the simulation is presented in Fig. 8 with instantaneous x-z slices of w, θ and r_v at 1300 LST. The spatial variation of net radiation is included in the figure to identify the areas shaded by cloud. Fig. 9 presents the total vertical transport of heat and moisture, which includes both the resolved ($_r$) and subfilter-scale ($_s$) components

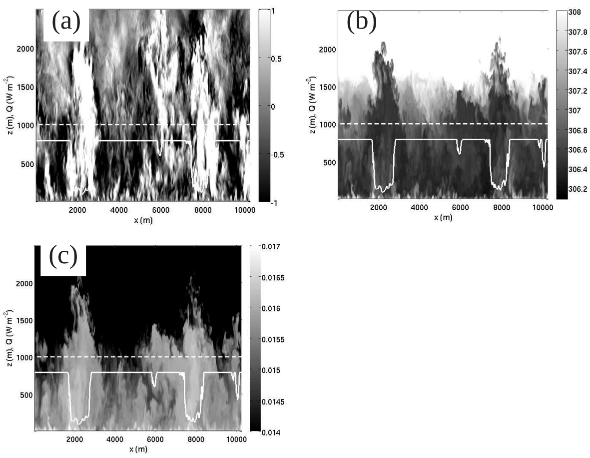

Figure 8: An instantaneous west-east vertical slice of (a) vertical velocity w (m s^{-1}), (b) θ (K), and (c) r_v (kg kg^{-1}) at 13:00 LST (shaded). The horizontal dashed white line indicates the mean boundary layer height over the domain and the continuous white line depicts the local net radiative forcing Q for this slice.

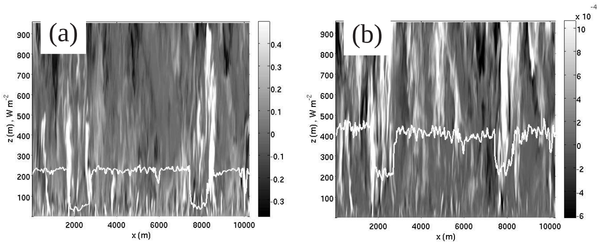

Figure 9: Same as Fig. 8 but for: (a) $w'\theta'$ (m s^{-1} K), and (b) $w'r_v'$ (m s^{-1} kg kg^{-1}) up to boundary layer height (grey shades). The white lines laid over top indicate: (a) surface heat flux H, and (b) latent heat flux LE along the vertical slice (W m^{-2}).

according to:

$$w'\theta' = (w'\theta')_r + (w'\theta')_s \tag{2}$$

$$w'r_v' = (w'r_v{}')_r + (w'r_v{}')_s \tag{3}$$

Contrary to the mean parameters (Fig. 8), instantaneous slices of total vertical flux (Fig. 9) do not clearly reveal the cloud root. In fact, without the overlaid surface fluxes, one would have difficulty locating the cloud root within the slices of local heat and moisture vertical transport. However, from the surface up to 200 m, regions of larger magnitude local heat and moisture fluxes can be seen (sometimes at both edges of the shaded areas, sometimes at just one edge). Therefore, the definition of a cloud root in the context of local heat and moisture fluxes remains unclear.

The sun being always at a zenithal position along the simulation, the simplest definition can be used in this

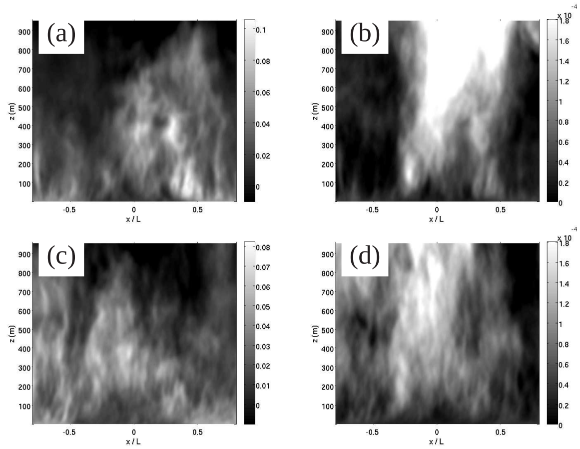

Figure 10: Averaged vertical slice of $w'\theta'$ (m s^{-1} K) and $w'r_v'$ (kg kg^{-1})) in cloud root (grey shades) along (a and b) and transverse (c and d) to the geostrophic wind. The average shaded extends between -0.5 $< x/L <$ +0.5, where L is the shaded area width along the slice.

study: the cloud root is defined as the air column above the shaded area.

In order to further generalize this result, Fig. 10 presents vertical slices of the simulation's average cloud root for clouds of larger than 1 km diameter and averagd over four different instantaneous 3D volumes sampled every 15 minutes between 12:00 and 13:00 LST. Prior to averaging, the fields were scaled spatially by their diameter (L) and shifted horizontally that the centroid of each cloud is located at a virtual origin (x/L = 0). The vertical slices presented in Fig. 10 therefore involve an average of more than 100 individual cloud-roots and the shaded area lies between -0.5 $< x/L <$ +0.5.

Very close to the ground, vertical slices aligned both along and transverse to the mean westerly wind (Fig. 10) confirm reduced vertical heat and moisture transport under the shaded area (*i.e.*, for -0.5 $< x/L <$ +0.5), which is in agreement with the surface fluxes beneath. Above the surface (from the ground to $0.2z_i$), atmospheric heat and moisture fluxes clearly reveal the surface heterogeneity's effect (Fig. 10). High magnitude heat and moisture vertical transport at the shaded area's edges (between 0 and 200 m) suggests enhanced vertical transport between the warm and relatively cold surfaces surrounding the shaded region, with this high bouyancy flux merging in the cloud root above 200 m.

Several numerical studies already showed that buoyant convection over heterogeneous surfaces occurs at the upwind edge of the warm patch (*e.g.*, Raasch and Harbusch, 2001; Patton et al., 2005; Courault et al., 2007, among others). However, the size of the surface heterogeneity in those studies were much larger than the cloud-induced shading under investigation here. It is also

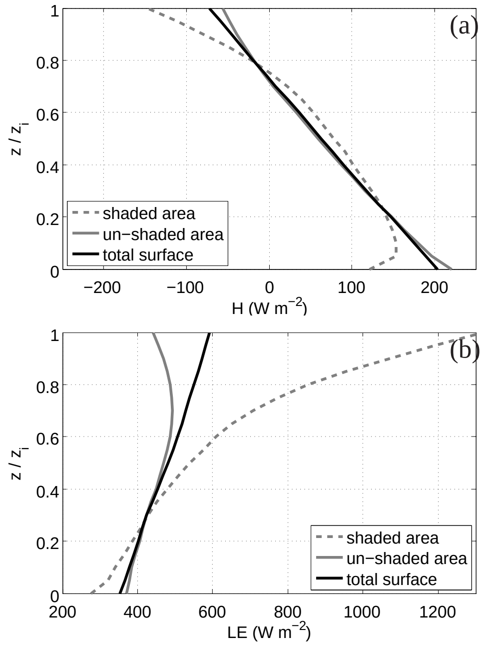

Figure 11: Sensible (a) and latent (b) heat flux against normalized height z/z_i for shaded area, un-shaded area and the total surface.

important to point out that those investigations also studied breeze circulations driven by horizontal temperature gradients, while in our case the dynamical circulation between shaded and un-shaded areas might be linked to the cloud-induced convection tending to generate convergence toward the cloud root.

The mean wind's effect is noticeable under the cloud base in Fig. 10a and b. The core with the upward transport of moisture under the cloud base is not centered but shifted downwind between $0 < x/L < +0.5$. On the contrary, the core of upward transport is notably centered in the transverse vertical slices (Fig. 10c and d). Heus and Jonker (2008) noticed that the upward core and the subsiding shells depends strongly on the wind shear.

To elaborate more fully on the influence of clouds on vertical transport, Fig. 11 presents the contribution to the total vertical flux F_T from shaded (F_s) versus un-shaded (F_{us}) areas, where F can be either H or LE. The profiles in Fig. 11 are averaged over the same 3D volumes as were used in Fig. 10.

If S_s and S_{us} describe the shaded area and un-shaded areas of the total surface S_T, respectively, F_s, F_{us} and F_T are linked by:

$$F_T = \frac{S_s}{S_T} F_s + \frac{S_{us}}{S_T} F_{us}. \tag{4}$$

The cloud-induced surface flux heterogeneity reduces the buoyancy flux from the surface up to $0.2 z_i$ over shaded areas; for example, the buoyancy flux at $0.1 z_i$ zi is reduced by 15 %. Between $0.2 < z/z_i < 0.8$, the cloud root exhibits stronger buoyancy flux than the surroundings, whereas above $0.8 z_i$ latent and sensible heat flux reveal the opposite behaviour (with a strong increase of latent heat flux and a slight decrease of sensible heat flux with height). Fig. 11b points out that the drying of the boundary layer through the cloud root (1300 W m^{-2}) (w' $>$ 0 and q' $>$ 0) is three times the drying occurring by entrainment of dry tropospheric air into the boundary layer (440 W m^{-2}) (w' $<$ 0 and q' $<$ 0).

5. Entrainment boundary layer with shallow clouds

Entrainment at the boundary layer's upper interface with the free troposphere participates fundamentally in heating and drying the boundary layer and tends to increase the surface evaporation (Heerwaarden et al., 2009). Beyond modifying the mean thermodynamical boundary layer characteristics, the downward dry and warm tongues coming from the PBL top can be detected at the surface (Lohou et al., 2010) on the turbulent time scales of temperature and moisture.

The entrainment rate is typically quantified by the ratio A defined as the magnitude of minus the buoyancy flux at the boundary layer top relative to the surface buoyancy flux (*e.g.*, Deardorff et al., 1980; Sullivan et al., 1998), which is derived from the horizontally-homogeneous buoyancy flux equation making a variety of assumptions. As such, entrainment rates also depend on conditions at boundary layer top, such as the inversion strength and wind shear (*e.g.*, Sullivan et al., 1998; Pino et al., 2003; Conzemius and Fedorovich, 2006; Canut et al., 2010, among others). From experiments, A is $\sim$ 0.25 (Deardorff et al., 1980, *e.g.*,), although significant controversy remains regarding the value of A (Fernando, 1991, *e.g.*,). The large variation of proposed values for A results partly from the method used to estimate the buoyancy flux at the boundary layer top, typically using linear extrapolation of the buoyancy flux profile up to the boundary layer top, but can also be attributed to A's dependence on the Reynolds, Prandtl and Peclet number of the fluid under consideration (*e.g.*, Jonker et al., 2012).

Fig. 11 reveals modifications to the upper portion of the mean vertical flux profiles in the shaded and un-shaded areas, which suggests that clouds modify the PBL-top buoyancy flux partitioning and potentially the entrainment rate (Fig. 1, point IV). Fig. 12 presents A's temporal evolution and its breakdown between sensible (A_θ) and latent (A_{r_v}) heat contributions for the simulation's duration, where the breakdown follows:

$$A = A_\theta (1 + 0.61 \langle r_v \rangle) + 0.61 \langle \theta \rangle A_{r_v}, \tag{5}$$

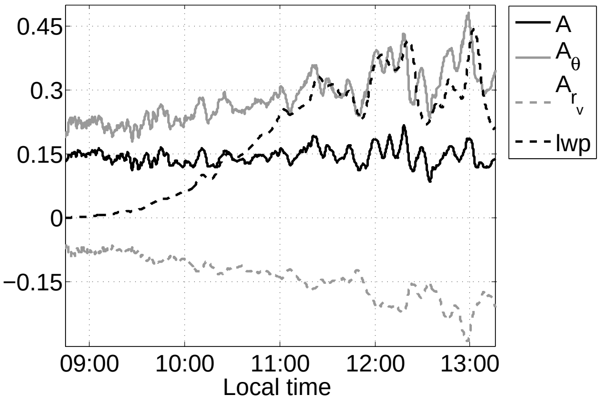

Figure 12: Temporal evolution of the entrainment rate A and its sensible A_θ and latent A_{r_v} contributions. The liquid water path (lwp, hg m^{-2}) is also included to show the cloud activity.

and $A_\theta = -\frac{\langle w'\theta'\rangle_{z_i}}{\langle w'\theta'_v\rangle_0}$, and $A_{r_v} = -\frac{\langle w' r_v'\rangle_{z_i}}{\langle w'\theta'_v\rangle_0}$, with subscripts z_i and 0 referring to the boundary layer top and surface levels, respectively. The liquid water path evolution indicates cloud layer development.

The temporal evolution of A_θ and A_{r_v} are obviously tied to the cloud activity at both diurnal and shorter time scales. One can discern from Fig. 12 that A_θ imposes smaller scale changes on A, while A_{r_v} is notably more smooth and generally follows the cloud activity development. In agreement with Fig. 11, the more active the cloud activity, the more the mean profile of latent heat flux over the domain tends to decrease its positive slope and the more the sensible heat flux tends to decrease its negative slope. However, the increase of buoyancy forcing from increasing latent heat flux below cloud base is generally compensated by a decrease of buoyancy forcing via decreasing sensible heat flux, leading to a generally constant A of around 0.15 along the simulation, confirming Nicholls and LeMone's (1980) result obtained using aircraft data during the GATE experiment. However, Fig. 12 reveals that A oscillates between 0.1 and 0.2, suggesting that the competing sensible and latent contributions do not completely compensate at short time scales. The entrainment rate tends to increase when cloud activity increases (as seen by increased liquid water path).

6. Discussion and conclusion

Shallow cumuli represent a large portion of the cloud cover over land, however their interaction with the surface energy balance (SEB) is poorly understood. One explanation for this lack of understanding lies in the difficulty to experimentally obtain estimates of the terms comprising the SEB terms. In this study, a large eddy simulation code is coupled with a land surface model to investigate the coupling between the surface and the atmosphere in the presence of shallow cumuli.

From a regional point of view, shallow cumuli are found to generate a 2 to 3% increase in evaporative fraction, no matter the soil type (ranging from pure loam to pure clay) or soil moisture regime. This increase results from the non-linear surface reponse to the cloud-induced reduction of the solar forcing. Latent heat flux decreases less ($\sim$ 5%) than the sensible heat flux (7 to 15%).

The limited reduction of evaporation by only 5% at regional scales results largely because evaporation increases locally in the shaded area such that evaporation is larger than the local net radiation, and is compensated by a sign change in soil heat flux. Therefore, when clouds pass overhead, heat moves toward the surface from deep in the soil and is consumed by evaporating surface water. The skin temperature decrease that leads to the sign change in ground heat flux also drives the sensible heat flux - which always represents one third of the local net radiation whether in or out of the shaded area. Therefore in cloudy conditions, the skin temperature is a critical parameter in the surface energy balance, where skin temperature undergoes important local and abrupt variations of more than 5 K.

As expected, the cloud-induced surface heterogeneities mainly result from the reduced solar forcing. The turbulence and secondary circulations associated with the cloud activity simply increase the flux variability at surface. However, it would be interesting to investigate wether or not this variability is involved in triggering cloud activity.

An investigation into the impact of cloud-induced surface heterogeneities on the vertical transfer of heat and moisture reveals that the buoyancy flux is modified by cloud-induced surface flux heterogeneity to heights above the surface layer (*i.e.*, up to $0.2z_i$). It is noteworthy that moving small-scale surface heterogeneities (with horizontal scale of about 1 km) lasting only a few minutes can impact vertical transfer to this height. On the other hand, higher fluxes are not observed above across all of the un-shaded area, but rather are found on the edges of the shaded area. These high buoyancy flux regions progressively coalesce above $0.2z_i$ to form the cloud's root. Cloud dynamics might become more important at this height, warranting futher future analysis.

Vertical sensible and latent heat flux profiles in the shaded and un-shaded areas differ notably, especially above $0.8z_i$ - where, the cloud root is defined by the atmospheric column above the shaded area. Between $0.8z_i$ and the cloud base, the cloud root strongly participates in drying and warming the boundary layer. These strong heat flux heterogeneities under the cloud base complicate airbone flux estimation by invalidating homogeneity and stationnarity hypotheses.

Despite sensible and latent flux modifications between the shaded and unshaded areas, the average buoyancy profile remains unchanged. The entrainment rate varies from 0.1 to 0.2 in response to cloud activity. Over the horizontal domain for long time scales, the cloud-induced latent heat flux increase to the buoyancy forcing determing the PBL's entrainment rate is largely compensated by a decrease in sensible heat flux. However, shallow cumuli activity increases the entrainment rate at shorter time scales.

acknowledgment:

The first author especially thank Paul Sabatier University (Toulouse III, France), the National Center for Atmospheric Research's (NCAR) Advanced Study Program, Geophysical Turbulence Program and MMM Division for supporting her visits to NCAR. The first author is endebted to Ned Patton and the Boundary Layer and Turbulence group for making her stay at NCAR a scientific and personal pleasure. We are particularly grateful to Peggy LeMone and Marie Lothon for their fruitful discussions and to Anil Kumar for his help in using HRLDAS and the 1D LSM. Computer facilities were provided by CALMIP (Calcul en Midi-Pyrénées, France) and NCAR. Edward Patton's support came from a combination of: 1) NCAR's Bio-hydro-atmosphere interactions of Energy, Aerosols, Carbon, H_2O, Organics & Nitrogen (BEACHON) project, and 2) the Center for Multiscale Modeling of Atmospheric Processes (CMMAP) at Colorado State University, NSF grant ATM-0425247 and contract G-3045-9 to NCAR. NCAR is sponsored in part by the National Science Foundation.

REFERENCES

Bellon, G. and B. Stevens, 2005: On Bulk Models of Shallow Cumulus Convection. *Journal of the Atmospheric Sciences*, **62**, 3286–3302.

Betts, A. K., 2007: Coupling of water vapor convergence, clouds, precipitation, and land-surface processes. *Journal of Geophysical Research*, **112 (D10)**, 1–14, doi:10.1029/2006JD008191.

Bony, S. and J.-L. Dufresne, 2005: Marine boundary layer clouds at the heart of tropical cloud feedback uncertainties in climate models. *Geophys. Res. Lett.*, **32 (20)**, 2–5, doi:10.1029/2005GL023851.

Bretherton, C. S. and S. Park, 2008: A New Bulk Shallow-Cumulus Model and Implications for Penetrative Entrainment Feedback on Updraft Buoyancy. *Journal of the Atmospheric Sciencesociety*, 2174–2193, doi:10.1175/2007JAS2242.1.

Brown, A., et al., 2002: Large-eddy simulation of the diurnal cycle of shallow cumulus convection over land. *Q.J.R. Meteorol. Soc.*, **128**, 1075–1093.

Canut, G., M. Lothon, and F. Lohou, 2010: Observation of entrainment at the interface between monsoon flow and the Saharan Air Layer. *Quarterly Journal of the Royal Meteorological Society*, **136 (AMMA special issue)**, 34–46, doi:10.1002/qj.471.

Chen, F., et al., 2007: Description and Evaluation of the Characteristics of the NCAR High-Resolution Land Data Assimilation System. *Journal of Applied Meteorology and Climatology*, **46 (6)**, 694–713, doi: 10.1175/JAM2463.1.

Conzemius, R. J. and E. Fedorovich, 2006: Dynamics of Sheared Convective Boundary Layer Entrainment. Part I: Methodological Background and Large-Eddy Simulations. *J. Atmos. Sci.*, **63**, 1151–1178.

Courant, R., K. Friedrichs, and H. Lewy, 1967: On the partial difference equations of mathematical physics. *IBM Journal of Research and Development*, **11 (2)**, 215–234.

Courault, D., P. Drobinski, Y. Brunet, P. Lacarrere, and C. Talbot, 2007: Impact of surface heterogeneity on a buoyancy-driven convective boundary layer in light winds. *Boundary-Layer Meteorology*, **124 (3)**, 383–403, doi:10.1007/s10546-007-9172-y.

Deardorff, J. W., 1970: A three-dimensional numerical investigation of the idealized planetary boundary layer. *Geophys. Astrophys. Fluid Dyn.*, **1 (3)**, 377–410.

Deardorff, J. W., 1980: Stratocumulus-capped mixed layers derived from a three-dimensional model. *Boundary-Layer Meteorol.*, **18**, 495–527.

Deardorff, J. W., G. E. Willis, and B. H. Stockton, 1980: Laboratory studies of the entrainment zone of a convectively mixed layer. *J. Fluid Mech.*, **100**, 41–64.

Fernando, H. J. S., 1991: Turbulent mixing in stratified fluids. *Annu. Rev. Fluid Mech.*, **23**, 455–493.

Golaz, J.-C., 2001: A large-eddy simulation study of cumulus clouds over land and sensitivity to soil moisture. *Atmospheric Research*, **59-60 (2)**, 373–392.

Hartmann, D. L., M. E. Ockert-Bell, and M. L. Michelsen, 1992: Hartmann.JC1992.pdf. *Journal of Climate*, **5**, 1281–1304.

Heerwaarden, C. C. V., A. F. Arellano, Jordi Vilà-Guereau Moene, and A. A. M. Holtslag, 2009: Interactions between dry-air entrainment, surface evaporation and convective boundary-layer development. *Q.J.R. Meteorol. Soc.*, doi:10.1002/qj.431.

Heus, T. and H. J. J. Jonker, 2008: Subsiding Shells around Shallow Cumulus Clouds. *Journal of the Atmospheric Sciences*, **65**, 1003–1018, doi: 10.1175/2007JAS2322.1.

Jiang, H. and G. Feingold, 2006: Effect of aerosol on warm convective clouds: Aerosol-cloud-surface flux feedbacks in a new coupled large eddy model. *Journal of Geophysical Research*, **111**, 1–12, doi: 10.1029/2005JD006138.

Jonker, H. J. J., M. van Reeuwijk, P. P. Sullivan, and E. G. Patton, 2012: Interfacial layers in atmospheric clear and cloudy boundary layers. *Turbulence, Heat and Mass Transfer 7*, Begell House, Inc., Palermo, Sicily, 1–12.

LeMone, M. a. and W. T. Pennell, 1976: The relationship of Trade Wind Cumulus Distribution to Subcloud Layer Fluxes and Structure. *Monthly Weather Review*, **104**, 524–539.

Lewellen, D. C. and W. S. Lewellen, 1996: Influence of Bowen Ratio on Boundary-Layer Cloud Structure. *Journal of the Atmospheric Sciences*, **53 (1)**, 175–187.

Lewellen, D. C. and W. S. Lewellen, 2002: Entrainment and Decoupling Relations for Cloudy Boundary Layers. *Journal of the Atmospheric Sciences*, **59 (2002)**, 2966–2986.

Lohou, F., B. Campistron, A. Druilhet, P. Foster, and J. P. Pages, 1998: Turbulence and coherent organizations in the atmospheric boundary layer: a radar-aircraft experimental approach. *Boundary-Layer Meteorology*, **86**, 147–179.

Lohou, F., F. Saïd, M. Lothon, P. Durand, and D. Serça, 2010: Impact of Boundary-Layer Processes on Near-Surface Turbulence Within the West African Monsoon. *Boundary-Layer Meteorology*, **136 (1)**, 1–23, doi: 10.1007/s10546-010-9493-0.

Moeng, C.-H., 1998: Stratocumulus-topped atmospheric planetary boundary layer. *Buoyant convection in geophysical flows*, E. J. Plate, E. Fedorovich, D. X. Viegas, and J. C. Wyngaard, Eds., Kluwer Academic Publishers, Dordrecht, The Netherlands, 421–440.

Moeng, C.-H., 2000: Entrainment Rate, Cloud Fraction, and Liquid Water Path of PBL Stratocumulus Clouds. *Journal of the Atmospheric Sciences*, **57**, 3627–3643.

Nicholls, S. and M. A. LeMone, 1980: The Fair Weather Boundary Layer in GATE: The Relationship of Subcloud fluxes and Structure to the Distribution and Enhancement of Cumulus Clouds. *Journal of the Atmospheric Sciences*, **37**, 2051–2067.

Nicholls, S., M. A. LeMone, and G. Sommeria, 1982: The simulation of a fair weather marine boundary layer in GATE using a three-dimensional model. *Q.J.R. Meteorol. Soc.*, **108**, 167–190.

Otles, Z. and J. A. Young, 1996: Influence of Shallow Cumuli on Subcloud Turbulent Fluxes Analyzed from Aircraft Data. *Journal of the Atmospheric Sciences*, **53 (5)**, 665–676.

Patton, E. G., P. P. Sullivan, and C.-H. Moeng, 2005: The Influence of Idealized Heterogeneity on Wet and Dry Planetary Boundary Layers Coupled to the Land Surface. *Journal of the Atmospheric Sciences*, **62 (7)**, 2078–2097, doi:10.1175/JAS3465.1.

Pino, D., J. V.-G. de Arellano, and P. J. Duynkerke, 2003: The contribution of shear to the evolution of a convective boundary layer. *J. Atmos. Sci.*, **60**, 1913–1926.

Raasch, S. and G. Harbusch, 2001: An Analysis Of Secondary Circirculations And Their Effects Caused By Small-Scale Surface Inhomogeneities Using Large-Eddy Simulation. *Boundary-Layer Meteorology*, **101 (1)**, 31–59, doi:10.1023/A:1019297504109.

Siebesma, A. P., 1998: Shallow cumulus convection. *Buoyant convection in geophysical flows*, E. J. Plate, E. E. Fedorovich, D. X. Viegas, and J. C. Wyngaard, Eds., Kluwer Academic Publishers, Dordrecht, The Netherlands, 441–486.

Siebesma, P. A., et al., 2003: A Large Eddy Simulation Intercomparison Study of Shallow Cumulus Convection. *Journal of the Atmospheric Sciences*, **60**, 1201–1219.

Slingo, A., 1990: Sensitivity of the Earth's radiation budget to changes in low clouds. *Nature*, **343**, 49–51, doi: 10.1038/343049a0.

Small, E. E. and S. A. Kurc, 2003: Tight coupling between soil moisture and the surface radiation budget in semi-arid environments: Implications for land-atmosphere interactions. *Water Resour. Res.*, **39 (10)**, 1–14, doi: 10.1029/2002WR001297.

Soares, P. M. M., P. M. A. Miranda, P. A. Siebesma, and J. Teixeira, 2004: An eddy-diffusivity/mass-flux parametrization for dry and shallow cumulus convection. *Q*, **8**, 3365–3383, doi:10.1256/qj.03.223.

Stechmann, S. N. and B. Stevens, 2010: Multiscale Models for Cumulus Cloud Dynamics. *Journal of the Atmospheric Sciences*, **67**, 3269–3285, doi: 10.1175/2010JAS3380.1.

Stephens, G. L., 2005: REVIEW ARTICLE Cloud Feedbacks in the Climate System: A Critical Review. *Journal of Climate*, **18**, 237–273.

Stevens, B., 2005: Atmospheric moist convection. *Ann. Rev. Earth Planet. Sci.*, **33 (1)**, 605–643, doi: 10.1146/annurev.earth.33.092203.122658.

Stevens, B., 2007: On the Growth of Layers of Nonprecipitating Cumulus Convection. *Journal of the Atmospheric Sciences*, **64 (8)**, 2916–2931, doi: 10.1175/JAS3983.1.

Stevens, B. and J.-L. Brenguier, 2009: Cloud controlling factors - Low clouds. *Clouds in the perturbed climate system*, J. Heintzenberg and R. J. Charlson, Eds., MIT Press, Cambridge, Massachusetts, 172–195.

Stull, R. B., 1988: *An introduction to boundary layer meteorology*. Kluwer Academic Publishers, Dordrecht, The Netherlands, 666 pp.

Sullivan, P. P., C.-H. Moeng, B. Stevens, D. H. Lenschow, and S. D. Mayor, 1998: Structure of the Entrainment Zone Capping the Convective Atmospheric Boundary Layer. *Journal of the Atmospheric Sciences*, **55 (19)**, 3042–3064, doi:10.1175/1520-0469(1998)055¡3042:SOTEZC¿2.0.CO;2.

Teidtke, M., W. Heckley, and J. Slingo, 1988: Tropical forecasting at ECMWF: The influence of physical parametrization on the mean structure of forecasts and analyses. *Quarterly Journal of the Royal Meteorological Society*, **114**, 639–664.

Tiedtke, M., 1989: A Comprehensive Mass Flux Scheme for Cumulus Parameterization in Large-Scale Models. *Monthly Weather Review1*, **117**, 1779–1800.

Webb, M. J., et al., 2006: On the contribution of local feedback mechanisms to the range of climate sensitivity in two GCM ensembles. *Climate Dynamics*, 17–38, doi:10.1007/s00382-006-0111-2.

Zhao, M. and P. H. Austin, 2005a: Life Cycle of Numerically Simulated Shallow Cumulus Clouds. Part I: Transport. *Journal of the Atmospheric Sciences*, **62 (5)**, 1269–1290, doi:10.1175/JAS3414.1.

Zhao, M. and P. H. Austin, 2005b: Life Cycle of Numerically Simulated Shallow Cumulus Clouds. Part II: Mixing Dynamics. *Journal of the Atmospheric Sciences*, **62 (5)**, 1291–1310, doi:10.1175/JAS3415.1.

Zhu, P. and B. Albrecht, 2003: Large eddy simulations of continental shallow cumulus convection. *Journal of Geophysical Research*, **108**, 1–18, doi: 10.1029/2002JD003119.